A High-Speed Charge Injection Circuit for Nanosecond-Scale Electrochemical Measurements

Junjun Huan
Electrical and Computer Engineering
University of Florida
Gainesville, FL, USA
Email: junjun.huan@ufl.edu

Jifu Liang
Electrical, Computer, and Systems Engineering
Case Western Reserve University
Cleveland, OH, USA
Email: jxl1265@case.edu

Nicholas Georgescu
Department of Chemistry
Case Western Reserve University
Cleveland, OH, USA
Email: nsg27@case.edu

Zhange Feng
Department of Chemistry and Biochemistry
Eastern Illinois University
Charleston, IL, USA
Email: zfeng@eiu.edu

Daniel Scherson
Department of Chemistry
Case Western Reserve University
Cleveland, OH, USA
Email: dxs16@case.edu

Soumyajit Mandal
Electrical and Computer Engineering
University of Florida
Gainesville, FL, USA
Email: soumyajit@ece.ufl.edu

***Abstract*—This paper describes a GaNFET-based high-speed charge injection circuit to study fast redox processes at electrode-electrolyte interfaces. The circuit allows the rates of electrode processes, which are much faster than those accessible with a conventional potentiostat, to be measured. It is able to inject charge across the interface within a few nanoseconds, and also to hold the potential generated across the cell following injection for up to 1 s without appreciable (less than 1%) decay. In addition, the circuit can still monitor the current flowing through the cell, as in a conventional potentiostat. Preliminary test results with both a dummy load and a custom two-electrode electrochemical cell confirm the functionality of the proposed circuit.**

***Index Terms*—electrode processes, electrochemical cell, charge injection, GaNFET**

I. Introduction

Electrochemical cells are widely used for studying redox reactions. An equivalent circuit model of a conventional three-electrode electrochemical cell is shown in Fig. 1(a), where WE, CE and RE represent the working, counter, and reference electrodes, respectively. Here and are the double-layer capacitance and Faradaic resistance of WE, respectively, while and are the equivalent quantities for CE. Finally, and are the solution resistances between WE and RE, and CE and RE, respectively. In many practical cells the CE is designed to be physically much larger than the WE, in which case its impedance can be neglected. Moreover, the RE is sometimes absent for simplicity, in which case we obtain the simplified two-electrode equivalent circuit shown in Fig. 1(b), where is the total solution resistance.

Various techniques have been developed to measure the rates of fast electron transfer processes at electrode-electrolyte interfaces within electrochemical cells [1]–[3]. Among the most popular is the potential step method, in which the cell current (assuming the RE is high-impedance) is measured just after the WE potential ( ) is suddenly changed [2], [3]. Conventionally, such potential steps (or other time-dependent potential functions) are generated by a potentiostat. A typical potentiostat (see Fig. 2) controls the potential of the WE with respect to that of the RE in accordance with the externally applied voltage through a negative feedback loop [3], while also measuring the current that flows between the WE and CE - either using a series resistor in series with CE (as shown here), or with a transimpedance amplifier (TIA) at WE. However, the closed-loop bandwidth of a potentiostat decreases as the time constant of the electrochemical cell (ignoring) increases, which causes the settling time of to increase. As a result, most commercial or research-based potentiostats are not designed for ultra-fast voltammetry (bandwidths over 10 MHz) or other types of fast perturbations [4]–[6].

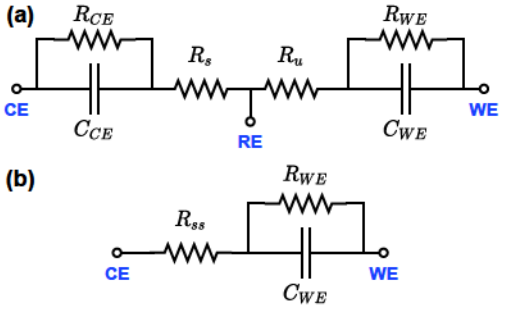

Fig. 1. Equivalent circuit models for (a) a complete three-electrode electrochemical cell, and (b) a simplified two-electrode electrochemical cell where the impedance of the counter electrode (CE) can be neglected.

This limitation can be explained by analyzing the closed-loop transfer function . We assume a typical three-electrode electrochemical cell model (Fig. 1(a)) but with the CE impedance and ignored for simplicity. We also assume that the op-amp is well-compensated, such that its transfer function can be modeled as an integrator ,

978-1-7281-9975-7/20/$31.00

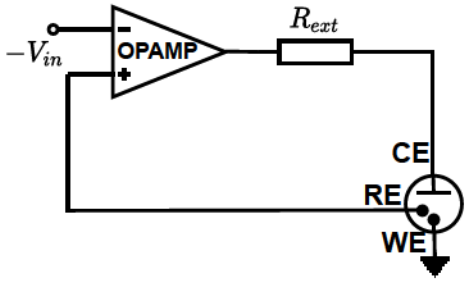

Fig. 2. Schematic of a three electrode cell controlled by a potentiostat. The circuit maintains the potential difference between the WE and RE at , where is an input voltage source, by applying current through CE. The latter is measured using a series resistor .

where and is the op-amp's gain-bandwidth product. A simple analysis [7], [8] then shows that

(1)

where and are the cell time-constants. This is a second-order low-pass response with a natural cut-off frequency , which decreases , as expected. Thus, the feedback loop speeds up the natural transient response of the cell by a speedup factor of approximately .

As an example, consider a cell with nF, , and k (these parameters are similar to those used in our experiments) and an op-amp with Mrad/s. The resulting Bode plot and step response of the potentiostat are shown in Fig. 3. The dB bandwidth is limited to 255 kHz as shown in Fig. 3(a), while the 10% settling time is 1.43 s. Bandwidth and settling time can be improved using a faster op-amp, as predicted by (1), but the weak (square-root) dependence of on implies that such improvements will be modest.

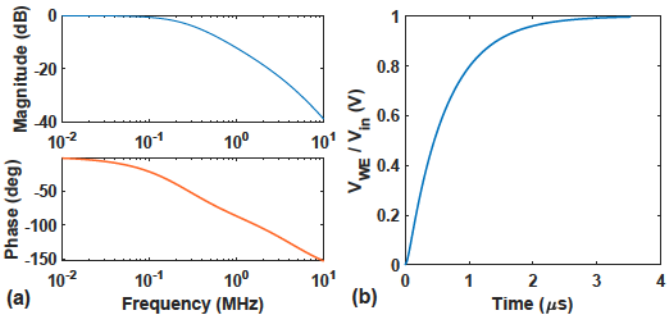

Fig. 3. (a) Bode plot and (b) step response of a typical potentiostat with nF, , k , and MHz.

As a result, typical potentiostats cannot accurately measure ultra-fast electrode processes, such as fast charge transfer reactions on sub- s timescales [9]. To overcome this limitation, this paper describes a high-speed charge injection circuit. Unlike closed-loop systems such as potentiostats, it interfaces the electrochemical cell in open loop by i) directly injecting charge into the cell to establish a potential step on WE; and ii) then maintaining the desired potential for a period of time to complete measurements. The proposed system also provides the flexibility of generating a potential step of various amplitudes and both polarities. Apart from these benefits, the proposed circuit still provides the useful functions of conventional closed-loop systems, including sensing both the initial charging current for the potential step and the Faradaic current due to redox reactions [9], [10].

II. Charge Injection Theory and Circuit Design

A. Electrochemical Cell Model

In our experiments, we consider a two-electrode cell with no RE. Thus, the device only contains two electrodes (WE and CE) immersed in an electrolyte. Also, we assume that the area of CE is much larger than that of WE, making its impedance negligible. In this case the cell can be represented by the simplified electrical equivalent circuit shown in Fig. 1(b) [3].

B. Theory of Charge Injection during Potential Steps

The circuit model shown in Fig. 1(b) indicates that the task of establishing a fast potential step to start electrode processes can be translated to the problem of fast charging of the WE double-layer capacitance in the presence of the solution resistance. More specifically, the goal is to charge the electrode capacitance to a desired potential (typically V) in times of the order of a few nanoseconds.

The charging method used here relies on applying a carefully-chosen waveform (shown in Fig. 4(a)) across a two-port electrochemical cell in an open-loop configuration, thus minimizing the effect of the cell time constant on circuit bandwidth. This waveform has two key features: i) a high initial injection voltage to provide the drop across ; and ii) a much smaller final voltage to set the final value of . Note that we assume is open-circuited on the timescale, i.e., that there is insufficient time for Faradaic reactions to occur during the potential step. In this case, a short pulse of cell current is generated during the injection period . This current linearly charges to during (see Fig. 4(b)), where . Thus, large injection voltages ( ) are needed to charge on short timescales (. However, typical high-speed DACs cannot generate such high voltages. Instead, in this paper we generate an approximation to the ideal waveform by discharging a small pre-charged capacitor into the cell.

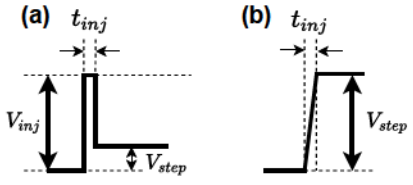

Fig. 4. (a) Ideal voltage waveform applied across a two-terminal electrochemical cell for fast charge injection, and (b) the resulting WE voltage.

Ignoring any parasitic capacitance C_{par} (e.g., due to the switches) at the injection electrode (assumed to be CE), a simple analysis shows that the cell current is now given by

$$I_{WE}(t) = -\frac{C_{inj}V_{HV}}{t_{inj}} e^{\frac{t}{\tau_1}} \left(e^{\frac{t_{inj}}{\tau_1}} - 1 \right) \approx -\frac{V_{HV}}{R_{ss}} e^{\frac{t}{\tau_1}}, \tag{2}$$

where V_{HV} is the pre-charge voltage, t_{inj} is the turn-on time of the discharge switch, $\tau_1 \equiv C_{inj}R_{ss}$, and the approximation on the right is valid when $t_{inj} \ll \tau_1$, which is generally the case. As a result, the WE voltage V_{WE} settles exponentially to its final value (determined by charge sharing), as

$$V_{WE}(t) = -\left(\frac{C_{inj}}{C_{WE}}\right) V_{HV} \left(1 - e^{t/\tau_1}\right). \tag{3}$$

Note that the settling time ($\approx 2.3\tau_1$ to 10%) is now set by $\tau_1 = C_{inj}R_{ss}$, which is much smaller than the cell time constant τ_{ss} since $C_{inj} \ll C_{WE}$. Thus, we can avoid the settling time constraints of a closed-loop potentiostat.

C. Charge Injection Circuit

The circuit schematic of the proposed high-speed charge injection circuit is shown in Fig. 5. Apart from the electrochemical cell under test, there are four main blocks in the proposed circuit, including sub-circuits for fast charging, sample-and-hold (S/H), and current measurement. The operation of the circuit consists of the following phases:

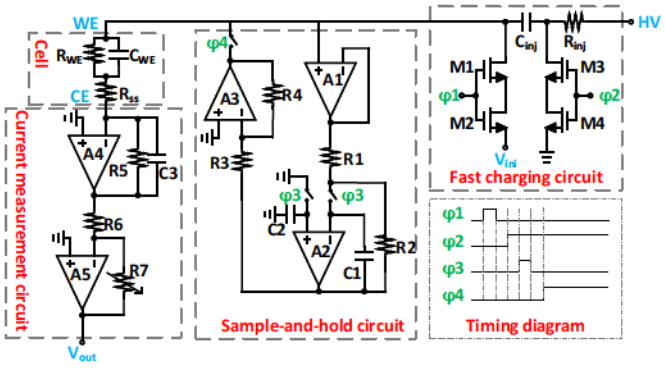

Fig. 5. Schematic of the high-speed charge injection circuit. $R_{inj} = 3$ kΩ; $C_{inj} = 10$ pF; $R_1 = R_2 = R_3 = R_4 = 150$ Ω; $R_5 = 20$ kΩ; $R_6 = 10$ Ω; $R_7 = 0 - 50$ kΩ; $R_{ss} = 100$ Ω; $R_{WE} = 1$ MΩ; $C_{WE} = 1$ nF; M_1-M_4 are GaNFETs.

1) Fast charging phase (ψ_1 and ψ_2): The key feature of the circuit is fast charging. Our charging sub-circuit uses GaNFET transistors (EPC2038, EPC) as the primary components for fast switching. The advantages of GaNFET transistors include low input capacitance, high breakdown voltage, low on-resistance, small footprint, and fast switching speed [11]. Therefore, GaNFET transistors are ideal for fast switching. Two of these transistors are connected back-to-back, as shown on the right-hand side of Fig. 5, to act as bidirectional (AC) switches.

During the ψ_1 phase, GaNFETs M_1 and M_2 are closed to set the initial condition V_{inj} of the cell. In addition, the injection capacitor (C_{inj}) is charged to a high voltage (e.g., $V_{HV} = 100$ V). In the ψ_2 phase, M_1 and M_2 are open, while M_3 and M_4 are closed. Since the GaNFETs have fast switching speed t_{inj}, the charge stored on C_{inj} is shared with C_{WE}. Therefore, C_{WE} is quickly charged to the desired voltage, as given by (3).

The final voltage on C_{WE} is given by

$$V_{final} = -\left(\frac{C_{inj}}{C_{WE}}\right) V_{HV} + V_{ini}, \tag{4}$$

where C_{inj} is the injection capacitance, C_{WE} is the electrode capacitor in the cell, V_{HV} is the high voltage and V_{ini} is the initial voltage used in the ψ_1 phase.

2) Voltage hold phase (ψ_3 and ψ_4): The potential across C_{WE} after fast charging needs to be maintained long enough to enable the current flowing through the cell to be measured. A sample-and-hold (S/H) circuit is used to achieve this goal, as shown in the middle of Fig. 5. Here, three operational amplifiers (op-amps) A_1-A_3 (AD8065, Analog Devices) are utilized. The voltage across capacitor C_{WE} is buffered by the unity-gain op-amp stage A_1. During the ψ_3 phase, the buffered voltage at the output of A_1 is amplified by the op-amp stage A_2 with a voltage gain of R_2/R_1. Here, R_1 and R_2 are selected to be equal so that the gain is unity. After the ψ_3 phase, this buffered voltage is stored on the capacitors C_1 and C_2, and the output of the A_2 is the voltage across C_{WE}. This voltage is maintained for a period of time, but the leakage current through the switches will eventually cause it to drift. During the ψ_4 phase, the output of A_2 is amplified in the op-amp stage A_3 with a voltage gain of R_4/R_3. Here, R_3 and R_4 are also equal in value. Therefore, the potential across C_{WE} after the fast charging operation can be sensed, stored, and then maintained by the proposed S/H circuit.

3) Current measurement phase: The current flowing through the electrochemical cell needs to be measured immediately following charging of C_{WE}. To this end, a current measurement circuit including two op-amp stages is utilized. A TIA stage (A_4) is used to convert $I_{WE}(t)$ to a voltage, and a programmable gain stage (A_5) is used to further amplify the converted voltage for better measurement sensitivity. The cell current can be calculated from the measured output voltage as

$$I_{WE}(t) = \frac{V_{out}(t)}{-R_5 \times G_1}, \tag{5}$$

where R_5 and $G_1 = -R_7/R_6$ are the transimpedance and voltage gain of the TIA and the inverting PGA, respectively. Note that while a linear TIA is shown in Fig. 5, in practice R_5 may need to be adapted in real-time to provide gain compression and thus maximize the TIA's dynamic range (DR). This is because the TIA needs high DR to measure both i) the large capacitive current during charge injection, and ii) the small Faradaic current during the hold phase.

III. Measurement Results

A prototype printed circuit board (PCB), shown in Fig. 6, was designed and constructed in order to experimentally verify the performance of the circuit. The board was tested with both an on-board dummy load representing an electrochemical cell,

as shown in Fig. 1(b), and an off-board electrochemical cell, as described later. The probes used in the experiment are high-speed passive probes with 1 GHz bandwidth. Before each experiment, the circuit was preset to zero initial conditions (V) for simplicity. However, other initial conditions can also be applied, e.g., to match the open-circuit voltage of the chosen electrochemical cell.

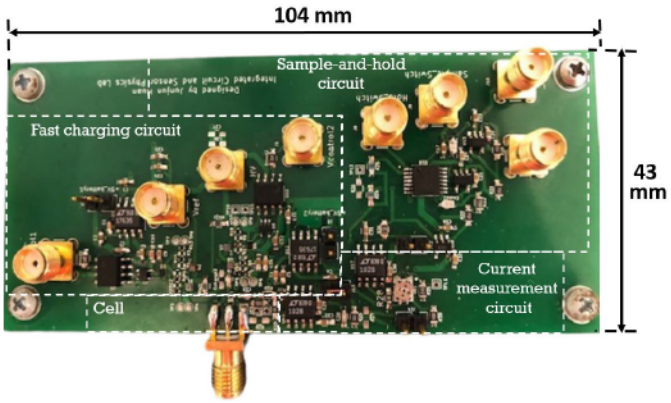

Fig. 6. Photograph of the printed circuit board.

A. Measurement Results with Different Gate Resistors

Since the GaNFET transistors are used for high-speed switching, an additional resistance is added in series with each gate terminal. The value of should be properly chosen to damp the ringing of the gate drive circuit while also maintaining low switching losses. Modeling the gate-source loop as a series circuit, the required resistance can be estimated as ——, where is the trace inductance of the gate-source loop, is the input capacitance of the GaNFET, and is the equivalent quality factor.

A series resistance of 20 was first selected to provide (i.e., a critically-damped condition), which minimizes voltage overshoot that can damage the gate oxide layer. Measured results for both positive and negative potential steps on a dummy load (1 nF in series with 100) using pF are shown in Fig. 7 and Fig. 8, respectively. In both figures, is the control signal applied at the gate of the GaNFETs (-) that triggers the charge injection process. was selected as 100 V, resulting a final voltage of 1 V based on (4). The measured results prove that the proposed circuit can inject both positive and negative charges to charge/discharge the dummy load to the desired value (V in this case) with extremely fast rise and fall times of around 3 ns and 5 ns, respectively (the settling time is several nanoseconds longer). The rise and fall times here are all calculated from 0 to 80% of the final voltage. The final voltage accuracy is over 90% of the theoretical value. However, it is also clear that significant voltage overshoot and voltage variations exist; this may cause breakdown of the double-layer capacitance of a real electrochemical cell, which is normally intolerant of voltages greater than 2 V.

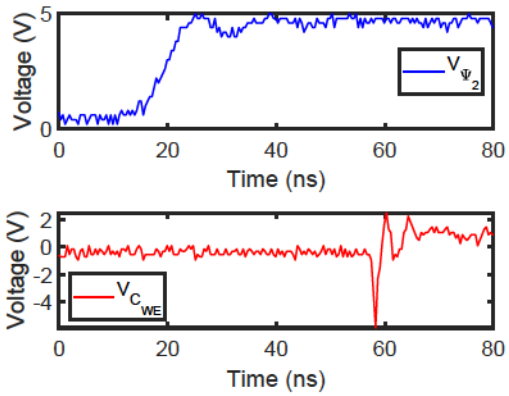

Fig. 7. Top: the control signal at the gates of discharges to start charge sharing between and . Bottom: the capacitor voltage rises to 80% of the desired value of 1 V in 3 ns for .

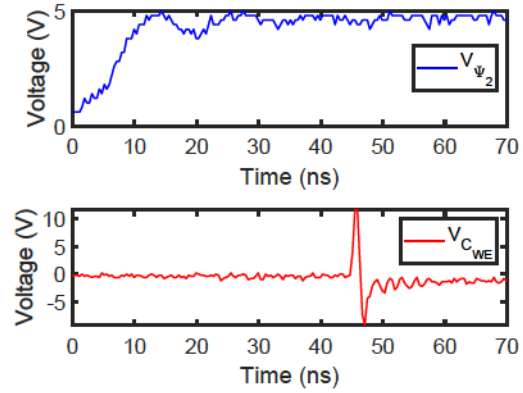

Fig. 8. Top: the control signal . Bottom: the measured capacitor voltage falls to 80% of the desired value of V in 5 ns for .

The simple solution to this issue is to use the same type of GaNFET but with higher to reduce the overshoot, at the cost of increased settling time. The best result during the experiments was obtained using , as shown in Fig. 9. The measured result has a clean positive voltage step of around 0.9 V to 1 V with no overshoot and voltage variations, and the settling time is around 31 ns. Again, the final voltage is within 10% of the theoretical value (1 V). Given such measured performance, the circuit is suitable for use with a real electrochemical cell.

B. Sample-and-Hold

Since leakage current from transistor-based switches is inevitable in the off-state, it is essential to use a S/H circuit to maintain the desired potential across . The same test conditions were used to verify the S/H circuit, and the measured results with and without the S/H are shown in Fig. 10. The S/H reduces the voltage decay to nearly zero within around 20 after an initial voltage drop of 150 mV (Fig. 10(a)). This loss is primarily caused by charge sharing with the parasitic capacitance. Still, stability of the steady state

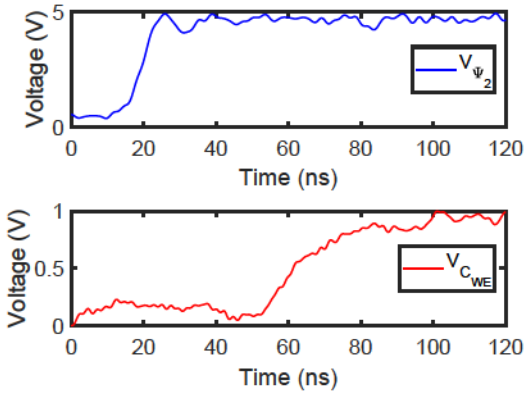

Fig. 9. Top: the control signal . Bottom: the measured capacitor voltage rises from 20% to 80% of the desired value of 0.95 V in about 22 ns without overshoot for . The 5% settling time is around 31 ns.

is greatly improved when compared to the potential decay rate of 10 mV/ s measured without the S/H (Fig.10(b)).

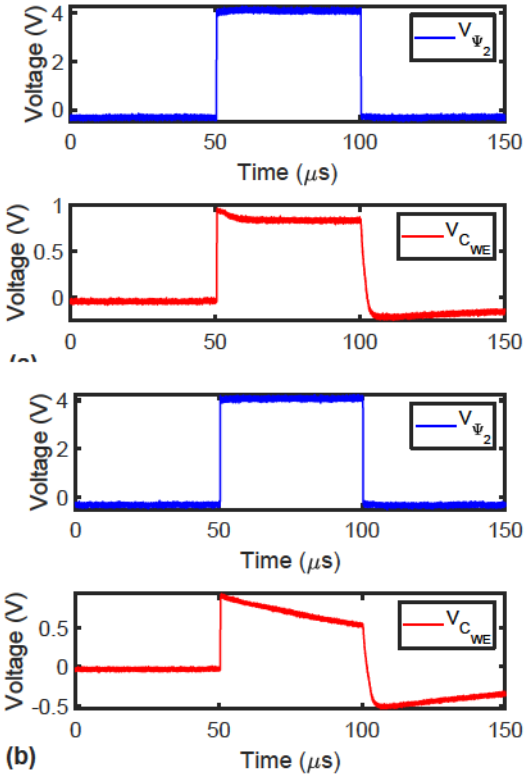

Fig. 10. Measured waveforms of the charge injection circuit (a) with S/H, and (b) without S/H. In each case, the top panel is the control signal , while the bottom panel is the capacitor voltage .

C. Current Measurement

Once the potential across the cell has been maintained, the current through the cell needs to be measured. When a large Faradaic resistor of M is used in the dummy load, the current through this load in the steady state should be 1 A when a 1 V potential is maintained across the cell. Fig. 11 shows the measured current in the cell, as inferred from the output of the current measurement circuit using (5). The measured value of 1 A matches the theoretical value. It is also noted that the reliable output voltage (stable current in the cell) can be obtained after the voltage settles to a steady value. The saturation observed before the steady state is due to the large charging currents that flow on s scales. Thus, a high-DR TIA design is required to measure both the charging and Faraday currents; this will be the focus of future work.

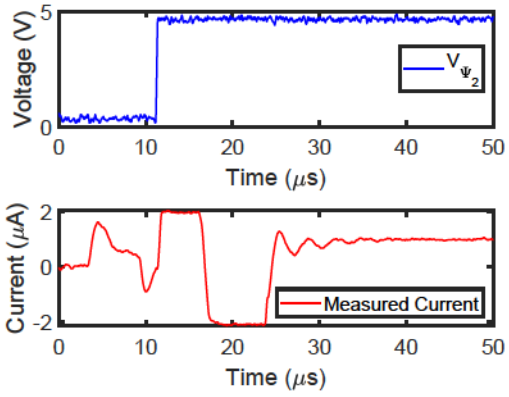

Fig. 11. Top: the control signal . Bottom: current flowing through the cell, as inferred from the output voltage of the current measurement circuit.

D. Experiments on an Electrochemical Cell

A simple off-board electrochemical cell was made to test the performance of the charge injection circuit. The gate series resistor was set to to minimize voltage overshoot and ringing, as described previously.

1) Test setup: Fig. 12(a) shows a photograph of the cell used for the experiments. A 50 m-diameter gold wire was used to create a disc-shaped WE, as follows. A glass capillary served as a holder for the gold wire, with its upper end completely open and the lower end only exposing the 2D cross-sectional area of the wire to the acid solution (see Fig. 12(b)). The CE was made by encircling the WE with a much larger gold wire (1.25 cm long, 0.25 mm diameter). This design ensures that the CE has at least larger area than the WE, such that its impedance can be neglected to fit the simplified model of Fig. 1(b).

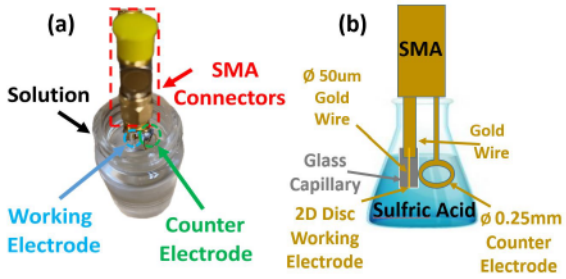

Fig. 12. (a) Photograph of the electrochemical cell used in the experiments. (b) Cross-sectional drawing of the cell.

2) Impedance measurements: The electrochemical cell was completed by filling the chamber shown in Fig. 12(b) with 0.1 M H_2SO_4. Its impedance was then measured with a vector network analyzer (Keysight E5061B). The goal was to identify the value of C_{inj} required to get a 1 V cell voltage after charge injection. The capacitance C_{WE} of the cell was measured to be ∼1 nF, which is in good agreement with the theoretical value of 0.4 nF obtained from the expression

$$C_{WE} = C_s \times A, \tag{6}$$

where C_s is the specific capacitance of a gold electrode immersed in the H_2SO_4 solution, and A is the interface area between the WE and the electrolyte [3].

The measured solution resistance $R_{ss} \approx 1.25\ k\Omega$ is also close to the theoretical value of ∼2 kΩ obtained from the well-known expression for a disk electrode, i.e.,

$$R_{ss} = \frac{1}{4k \times r}, \tag{7}$$

where k is the conductivity of the 0.1 M H_2SO_4 solution, and $r = 50\ \mu$m is the radius of the working electrode [3].

3) Charge injection results: While testing the circuit using the electrochemical cell, note that only the voltage between the WE and CE can be measured (i.e., the voltage across C_{WE} cannot be directly measured, unlike in the earlier experiments). The measured charge injection waveform is shown in Fig. 13. It is similar to the theoretical waveform shown in Fig. 4(a), thus confirming that the circuit can charge the cell to 1 V and hold the voltage for a long time. Note that the rise and settling times timescale are significantly longer than with the on-board dummy load. This is due to the high solution resistance R_{ss}, which reduces the current supplied to C_{WE} during charge injection (see (2)) and also increases the settling time constant $\tau_1 = C_{inj}R_{ss}$. Nevertheless, the measured 2% settling time of 127 ns is: i) in agreement with the theoretical value of $\approx 4\tau_1 = 50$ ns for this cell; and ii) significantly smaller than for a typical potentiostat (e.g., 1.43 μs using an op-amp with $f_a = 10$ MHz, as shown in Fig. 3).

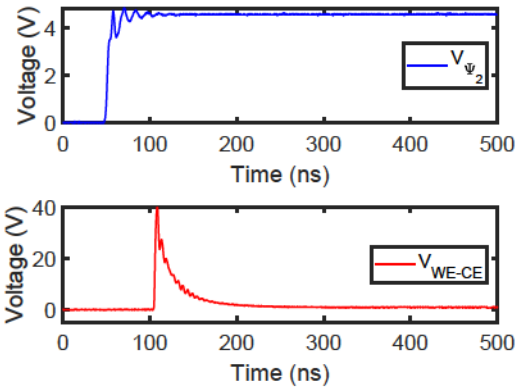

Fig. 13. Top: the control signal $V_{\psi 2}$. Bottom: the measured cell voltage $V_{WE\ CE}$ settles to within 2% of the desired value (1 V) in 127 ns. The peak voltage overshoot of ∼40 V is where charge injection takes place.

Settling times using the charge injection circuit can be further reduced by either using a cell with much lower R_{ss} or by using a smaller capacitor C_{inj}. However, the latter solution makes the circuit more sensitive to board-level parasitics.

IV. Conclusion

This paper has proposed a high-speed charge injection circuit for electrochemical experiments. The circuit was tested with both an on-board dummy load (modeling the equivalent circuit of a real electrochemical cell) and also a home-made electrochemical cell. Measured results prove that the overall performance of the charge injection circuit is excellent with extremely low injection times of around 10 ns and 30 ns for a response with and without voltage overshoot, respectively; $>$ 90% accuracy of the final voltage after charging; low voltage drop of ∼150 mV when using a S/H to hold the final voltage for tens of μs; and accurate on-board current measurement functionality. Future work will focus on testing the proposed circuit with optimized electrochemical cell designs. To obtain good experimental results, real cell parameters will be measured to ensure accuracy. Next, the component values of the proposed system (e.g., the injection capacitance) will be updated accordingly. An optical system like the one described in [9] will then be used to monitor the resulting potential across the working electrode-electrolyte interface.

Acknowledgement

This project was partially funded by the National Science Foundation under award CHE 1808592

References

[1] J. G. Goldsmith, "Modern analytical chemistry, 1st edition (Harvey, David)," *Journal of Chemical Education*, vol. 77, no. 6, p. 705, 2000.

[2] P. Kissinger and W. R. Heineman, *Laboratory Techniques in Electroanalytical Chemistry, revised and expanded*. CRC press, 1996.

[3] A. J. Bard and L. R. Faulkner, *Electrochemical Methods: Fundamentals and Applications*. Wiley, 2nd ed., 2001.

[4] D. E. Tallman, G. Shepherd, and W. J. MacKellar, "A wide bandwidth computer based potentiostat for fast voltammetry at microelectrodes," *Journal of Electroanalytical Chemistry and Interfacial Electrochemistry*, vol. 280, no. 2, pp. 327 – 340, 1990.

[5] A. Bard and M. Stratmann, *Encyclopedia of Electrochemistry*. No. v. 7, pt. 1 in Encyclopedia of Electrochemistry, Wiley-VCH, 2006.

[6] L. D. Ha, K. Park, B.-Y. Chang, and S. Hwang, "Implementation of Second-Generation Fourier Transform Electrochemical Impedance Spectroscopy with Commercial Potentiostat and Application to Time-Resolved Electrochemical Impedance Spectroscopy," *Analytical Chemistry*, vol. 91, pp. 14208–14213, NOV 19 2019.

[7] R. R. Schroeder and I. Shain, "The application of feedback principles to instrumentation for potentiostatic studies," *Instrumentation Science & Technology*, vol. 1, no. 3, pp. 233–259, 1969.

[8] D. Britz, "iR elimination in electrochemical cells," *Journal of Electroanalytical Chemistry and Interfacial Electrochemistry*, vol. 88, no. 3, pp. 309–352, 1978.

[9] R. S. Robinson and R. L. McCreery, "Submicrosecond spectroelectrochemistry applied to chlorpromazine cation radical charge transfer reactions," *Journal of Electroanalytical Chemistry and Interfacial Electrochemistry*, vol. 182, no. 1, pp. 61 – 72, 1985.

[10] A. Michael and L. Borland, *Electrochemical Methods for Neuroscience*. Frontiers in Neuroengineering Series, CRC Press, 2006.

[11] A. Lidow, J. Strydom, M. de Rooij, and D. Reusch, *GaN Transistors for Efficient Power Conversion*. Wiley, 2014.